Research Article

Haider Raza, Sohail Faroog, Sobia Sattar, Sadique Rehman, Aamir Faroog*, Muhammad Kamran, Mansoor Alshehri, and Nehad Ali Shah

Melting phenomenon of thermally stratified MHD Powell-Eyring nanofluid with variable porosity past a stretching Riga plate

https://doi.org/10.1515/rams-2024-0020 received September 24, 2023; accepted April 15, 2024

Abstract: Recently, experts have become particularly interested in the treatment of disorders caused by magnesium shortage. Hypomagnesemia is produced by a magnesium deficit in the blood, which is an additional stimulation for different diseases such as vomiting, drowsiness, nausea, loss of appetite, and so on. To compensate for this shortage, magnesium is injected as a nanoparticle in the blood (base fluid). The properties of these magnesium nanoparticles specifically their size, dispersion, and surface characteristics are crucial for optimizing their bioavailability and therapeutic efficacy. Advanced material characterization techniques ensure the stability and enhanced performance of these nanoparticles in the physiological environment. Based on these applications, the current research aims to address magnesium deficiency via Powell-Eyring nanofluid flow distorted by the linearly stretchable sheet in the region of the stagnation point. Linear thermal stratification, viscous

dissipation, and Joule heating are used to reveal the heat transport features. The magnetic field is applied to the nanofluid at an angle α to further control the fluid dynamics and nanoparticle behavior. Transformations are used to create a set of dimensionless governing equations. Comparative graphs are used to explain the physical behaviors of temperature and velocity fields, demonstrating how material properties impact fluid dynamics. The well-known convergence method (homotopy analysis method) is used to solve the model by comparing graphs.

Keywords: melting rheology, thermal stratification, Powell-Eyring nanofluid, analytical solution, mixed convective flow

Nomenclature

а

 B_0

stretching rate

magnetic field strength

* Corresponding author: Aamir Farooq, Department of Mathematics, Zhejiang Normal University, Jinhua, 321004, China, e-mail: aamirf88@yahoo.com Haider Raza: Department of Mathematics, COMSATS University Islamabad, Wah Campus, Pakistan, e-mail: icz4260@gmail.com Sohail Faroog: School of Chemical, Biological, and Environmental Engineering, Oregon State University, Corvallis, Oregon, 97331, United States of America, e-mail: sohailfarooq819@gmail.com Sobia Sattar: Department of Mathematics, COMSATS University Islamabad, Wah Campus, Pakistan, e-mail: sobia4060@gmail.com Sadique Rehman: Division of Mathematical and Physical Sciences, Kanazawa University, Kakuma, Kanazawa, 920-1192, Japan, e-mail: sadique@stu.kanazawa-u.ac.jp Muhammad Kamran: Department of Mathematics, COMSATS University Islamabad, Wah Campus, Pakistan, e-mail: getkamran@gmail.com Mansoor Alshehri: Department of Mathematics, College of Sciences, King Saud University, P.O. Box 2455, Riyadh, 11451, Saudi Arabia, e-mail: mhalshehri@ksu.edu.sa Nehad Ali Shah: Department of Mechanical Engineering,

inertia coefficient $C_{\rm b}$ skin friction coefficient $C_{\rm f}$ specific heat $C_{\rm p}$ d, d_1 dimensional constants Ec Eckert number dimensional constants e_1, e_2 Ha magnetic parameter applied current density in electrodes h_0 width of magnets between electrodes j_1 K thermal conductivity of nanofluid K(y)variable permeability of porous medium melting parameter M magnetization of the permanent magnets m_0 local Nusselt number Nu_x nf nanofluid Pr Prandtl number Q_0 heat source stratified thermal factor S_1 T temperature T_{∞} surrounding temperature

Sejong University, Seoul 05006, Republic of Korea,

e-mail: nehadali199@yahoo.com

2 — Haider Raza et al. DE GRUYTER

 T_0 reference temperature $T_{\rm m}$ melting temperature U_{w} stretching velocity U_{∞} free stream velocity velocity components u, v displacement in Cartesian coordinate *x*, *y* system dynamic viscosity μ $B_0\beta$, C_1 material parameters $\beta(y)$ variable porosity electrical conductivity σ λ latent heat of fluid density ρ α angle of inclination θ dimensionless temperature

1 Introduction

similarity variable

η

Studies of flow models for non-Newtonian liquids, which are widely used in manufacturing and industrial settings have gained the attention of scholars and researchers in recent years. Various industries, including fusion reactors, planetary research, metallurgy, paper manufacture, oil engineering storage, polymeric solutions, nuclear power, chemical production, bioengineering, geophysics, and pharmaceuticals, have utilized non-Newtonian liquids for a variety of purposes. Many researchers have explored non-Newtonian flow phenomena in a variety of geometries because of the many technological and industrial applications that these phenomena have. One benefit of the non-Newtonian fluid model proposed by scientists Powell and Evring in 1944 is that it behaves like a viscous fluid at high shear rates. The model is drawn from the kinetic theory of gases rather than empirical formulas. Jabeen et al. [1] studied the crucial role that stratification phenomena caused by an inclined sheet that is stretched linearly play in Powell-Eyring fluid flow. For instance, the Powell-Eyring model is a popular rheological model used to explain the flow characteristics of non-Newtonian fluids, especially those that behave as shear-thinning. Based on the idea of a yield stress fluid, this model allows material to flow only upon exceeding a specific threshold stress, or yield stress. Under this limit, the substance exhibits no flow and behaves like a solid. Lund et al. [2] investigated the various solutions for the unsteady flow of a Cu-Al₂O₃/ water-based hybrid nanofluid within a Darcy-Forchheimer porous medium, considering the impacts of Joule heating and viscous dissipation. Rehman et al. [3] concentrated on the features of the melting heat phenomena in the PowellEyring fluid flow that was distorted around the stagnation point by the linearly stretchable sheet. In the presence of a magnetic field, Hatami et al. [4] performed analytical and numerical simulations of heat transfer and flow analysis for a non-Newtonian third-grade nanofluid flow in a porous medium in a hollow vessel. The addition of gold (Au) nanoparticles to blood is thought of as the base third-grade non-Newtonian fluid. Numerical analysis is performed on a three-dimensional non-Newtonian nanofluid flow with nonlinear thermal radiation and heat absorption. With the above in mind, Tarakaramu et al. [5] considered the nonlinear heat absorption and radiation on porous stretched sheets. Shahzad et al. [6] demonstrated a non-Newtonian cross-fluid that is asymmetrically flowing over a radially expanding sheet. The flow of nanofluid is additionally represented by Buongiorno model for tiny particles, a physical problem. Using ethylene glycol as a base fluid and a non-Newtonian Maxwell fluid model, Jeelani and Abbas [7] investigated how to improve energy/heat transfer by dispersing copper and alumina nanoparticles in a cylindrical shape. The present work investigates the effects on a Maxwell hybrid nanofluid of plate suction. MHD, and solar radiation.

Contemporary scientists are increasingly drawn to nanotechnology due to the remarkable optical, electrical, and chemical characteristics exhibited by materials at the nanoscale. Recent advancements have facilitated the dispersion of nanoparticles within conventional heat-transfer fluids, including water, ethylene glycol, and motor oil, thereby introducing a novel category of highly efficient heat transfer liquids. Vinodkumar Reddy et al. [8] explored the MHD stagnation point flow of Williamson hybrid nanofluid across a stretching sheet in a porous medium, incorporating a heat source and chemical reaction. Further, Al-Farhany et al. [9] conducted a numerical analysis on mixed convective double diffusion in a tilt curvilinear lid-driven cavity using a Fe₃O₄-water-based nanofluid, considering the influence of an inclined magnetic field. Further applications of nanofluid discussed in previous literature [10–12]. Furthermore, Gorla et al. [13] provided a boundary layer analysis for mixed convection across a vertical wedge in a porous media saturated with nanofluid. A laminar, steady, natural convection boundary-layer flow was investigated by Chamkha and Rashad [14] over a permeable vertical cone contained in a porous media saturated with a nanofluid, with uniform lateral mass flux. Khan et al. [15] performed a computational investigation into the boundary layer flow and heat transfer characteristics of fractional Maxwell viscoelastic nanofluids and their hybrids on a porous vertical surface. Hussain et al. [16] employed response surface methodology to conduct a sensitivity analysis of the flow of gold nanoparticles in blood over a spinning disc while accounting for slippage, Joule heating, nonlinear thermal radiation, and viscous dissipation. Rafigue et al. [17] investigated the impact of numerous variables, including thermal stratification, viscous dissipation, velocity slip conditions, ternary hybrid nanofluid, MHD stagnation point flow, and variable viscosity, on coolant applications. Lone et al. [18] focused on the Casson nanofluid's gyrotactic bioconvection flow on a bidirectional linear stretching sheet while considering the effects of an angled magnetic field.

Stratification, both in industrial processes and natural settings, plays a crucial role in various operations. It occurs due to changes in concentration, temperature, or the presence of fluids with differing densities within fluid systems. Double stratification arises when mass and heat transfer operations occur simultaneously. In natural bodies of water such as seas and reservoirs, thermal layering manifests as stratification, while salinity gradients are observable in rivers, canals, groundwater dams, and oceans. Environmental contexts and numerous commercial food preparation and production activities also feature heterogeneous mixes. Gravity-induced density variations significantly influence the mixing and dynamics of such heterogeneous liquids. Anoxic conditions may arise from biological processes, such as when thermal stratification limits the oxygen supply to deeper water levels in reservoirs. Overall, stratification largely regulates the temperature and concentration levels in ponds and lakes, demonstrating its critical role in various natural and industrial processes. Kandasamy et al. [19] examined the flow of MHD nanofluid on a porous plate that was oriented vertically. He used the RK technique to study temperature declines with an enhanced thermal stratification parameter. Ahmad et al. [20] analyzed the unstable bio-convective hybridized micropolar nanofluid flow across a vertically increasing surface under stratification circumstances. Rehman et al. [21] evaluated the Casson fluid flow that emerges from a stretched cylinder with heat generation coming from both convection and thermal stratification. Jabeen et al. [22] highlighted the properties of mixed convection in Powell-Eyring fluid under stretchy sheet deformation with an inclined inclination. The features of heat transfer are shown by thermal stratification. To shed light on the nature of mass transfer, fluid viscosity stratification and first-order chemical processes are also taken into consideration. Bilal et al. [23] presented interesting aspects of thermal stratification in order to explore the flow properties of the Carreau fluid. Flow field equations are derived from the combination of infinite shear rate viscosity and magnetic field effects.

The flow of conductive fluids is studied in MHDs. Its use is broad and encompasses disciplines such as cosmic plasmas and liquid metals. Applications for this technology include MHD pumps and power generators, electrostatic precipitation, petroleum industry use, crude oil purification, aerodynamic heating, geophysics exploration, plasma physics, and fluid droplet dispersion [24]. Krishna et al. [25] examined the behavior of radiative unsteady MHD flow in a non-Newtonian Casson hybrid nanofluid that is both incompressible and viscous. This flow occurs over a surface moving vertically with exponential acceleration, extending infinitely. Additionally, slip velocity and rotation effects were taken into account within the analysis. Madhu et al. [26] considered the investigation of the phenomenon involving the unsteady MHD boundary layer flow of a non-Newtonian Maxwell nanofluid over a stretching surface, incorporating thermal radiation. Hafez et al. [27] investigated the electroosmosis-modulated Darcy-Forchheimer flow of Casson nanofluid over stretching sheets, considering the effects of Newtonian heating. Bhadauria et al. [28] examined the thermal instability of tri-hybrid Casson nanofluid within various enclosures featuring a thermally radiating saturated porous medium. Felicita et al. [29] explored the mixed convective flow of Casson nanofluid in a microchannel, analyzing the impact of couple stresses and irreversibility. Kulkarni and Shankar [30] conducted a numerical study on the mixed convective flow of Williamson nanofluid over a stretching/shrinking wedge, considering the influence of a chemical reaction parameter and liquid hydrogen diffusion. Reddy et al. [31] investigated the effects of radiation, velocity, and thermal slips on the MHD boundary layer flow, involving heat and mass transport of Williamson nanofluid through a porous medium. Akram and Afzal [32] researched the impacts of thermal and concentration convection and an induced magnetic field on the peristaltic flow of Williamson nanofluid in an inclined uniform channel.

Assessing the effect of Powell-Evring nanofluid in a state of stagnation moving under an angled magnetic field is the main goal of this work. The base fluid is blood, and magnesium (Mg) nanoparticles are added to it. Since this fluid model exhibits the characteristics of shear-thinning fluids, blood was used here to simulate Powell-Eyring fluid. Due to the fact that the blood exhibits shear thinning characteristics with rising shear stress, it is even more important to pay notice to this aspect. For instance, to pump blood into the arteries, the heart applies additional shear stress to the blood. Shear thinning, which prevents clots from forming in the veins, is the reason for its swift, clot free flow. The impacts of viscous dissolution, Joule heating, and a more realistic aspect of melting the transfer of heat are replaced in order to examine heat transmission. The melting point of the skin on the foot is between 0 and 10°C, while the fat inside the body melts between 30 and 35°C. The melting point of several different kinds of lipids is

greater than the average human body temperature of 37°C. In the current work, we used blood as a base fluid and added magnesium particles to raise the temperature and act as a temperature regulator. Blood temperature is greater than the walls of veins. As a result, the fats within the vein wall begin to melt as the temperature rises. To examine the true image of blood flow in veins, particularly in the aorta, the melting condition is therefore favored in this investigation [33]. Linear stratification is used to examine heat transmission in a better way. First, the necessary transformations are used to create the resultant non-dimensional governing equations, and then the technique of homotopy analysis is used to identify convergent solutions. Various parameters are depicted in graphical form to display temperature and velocity profiles. Table 1 demonstrates the variations between the present work and published literature.

2 Statement of the problem

Let us consider the steady, incompressible, MHD Powell-Eyring nanofluid flow with variable porosity along with a stretchable Riga plate close to the stagnation point. The magnetic field is applied at a certain angle α . The magnetic Reynolds number is supposed to be small; therefore, the induced magnetic field is neglected while the ion slips and Hall effects is assumed to be negligible. The porous medium is transparent and in thermal equilibrium state with fluid. Melting rheology is taken to improve the heat transport characteristics. In this phenomenon, the ambient temperature T_{∞} is smaller than the fluid temperature $T_{\rm m}$, i.e., $(T_{\rm m} > T_{\infty})$. Thermal slip, Joule heating, viscous dissipation, and thermal stratification impact are grasped here to increase the heat transfer. We supposed that the fluid phase and nanoparticles are in thermal equilibrium state. To treat disorders, magnesium nanoparticles are plucked into a base fluid (blood) to recover the diseases caused by the deficiency of magnesium in the human body. The problem's geometric representation is illustrated in Scheme 1. Using normal boundary layer approximations, one can achieve the governing equations, which are shown as follows [3]:

$$\frac{\partial u}{\partial x} + \frac{\partial v}{\partial y} = 0,\tag{1}$$

$$\rho_{\rm nf} \left[u \frac{\partial u}{\partial x} + v \frac{\partial u}{\partial y} \right] = U_{\infty} \frac{\mathrm{d}U_{\infty}}{\mathrm{d}x} + \left[\mu_{\rm nf} + \frac{1}{\beta C_1} \right] \frac{\partial^2 u}{\partial y^2}$$

$$- \frac{1}{2\beta C_1^3} \left[\frac{\partial u}{\partial y} \right]^2 \times \frac{\partial^2 u}{\partial y^2} - \frac{\mu_{\rm nf} \beta(y)}{K(y)} u$$

$$- \frac{\rho_{\rm nf} C_1 \beta^2(y)}{\sqrt{K(y)}} u^2 - \sigma_{\rm nf} B_0^2 \sin^2(\alpha) (u$$

$$- U_{\infty}) + \frac{\pi m_0 h_0}{8} e^{\left[-\frac{\pi}{j_1} \right]^y},$$
(2)

$$(\rho C_{\rm p})_{\rm nf} \left[u \frac{\partial T}{\partial x} + v \frac{\partial T}{\partial y} \right]$$

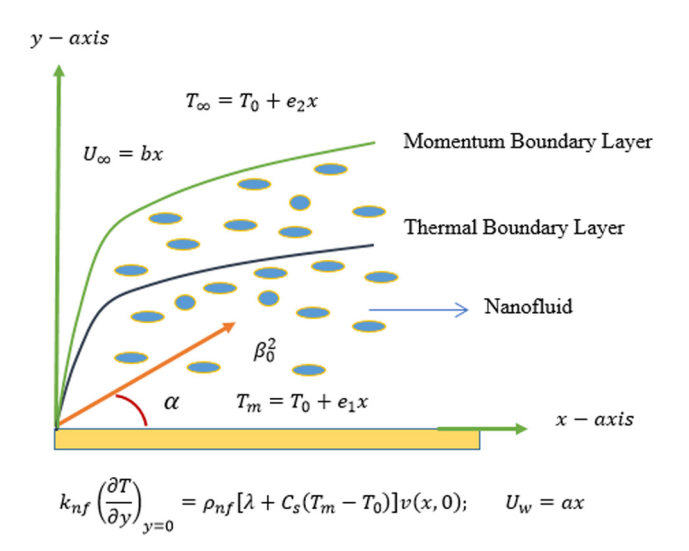
$$= K_{\rm nf} \frac{\partial^2 T}{\partial y^2} + \left[\mu_{\rm nf} + \frac{1}{\beta C_1} \right] \left(\frac{\partial u}{\partial y} \right)^2 - \frac{1}{6\beta C_1^3} \left(\frac{\partial u}{\partial y} \right)^4$$

$$+ \sigma_{\rm nf} B_0^2 \sin^2(\alpha) (u - U_{\infty})^2 + Q_0 (T - T_m).$$
(3)

According to the boundary conditions executed [3],

$$u = U_w(x) = ax, \quad T = T_m \text{ as } y \to 0,$$

$$u = U_\infty(x) = bx, \quad T = T_\infty \text{ as } y \to \infty$$
(4)



Scheme 1: Geometry of the problem.

Table 1: The novelty of present work

Effects	Nisar <i>et al.</i> [34]	Rehman <i>et al.</i> [3]	Saif <i>et al.</i> [35]	Farooq and Javed [36]
Melting heat transfer	No	Yes	No	Yes
Thermal stratification	No	Yes	No	Yes
Variable porosity and permeability	No	No	Yes	No
Stagnation point	No	Yes	No	Yes
Inclined magnetic field	No	Yes	Yes	No
Nanofluid	Yes	No	No	Yes

$$K_{\rm nf} \frac{\partial T}{\partial y} \bigg|_{y=0} = \rho_{\rm nf} [\lambda + C_{\rm s}(T_m - T_0)] v(x, 0), \tag{5}$$

where

DE GRUYTER

$$T_m = T_0 + e_1 x$$
, $T_\infty = T_0 + e_2 x$.

where u and v are the components of the velocity in horizontal and vertical directions respectively. $U_{\rm w}$ is the stretching velocity, U_{∞} is the free stream velocity, T is the temperature of a fluid, T_0 is the reference temperature, $T_{\rm m}$ is the temperature of the melting surface, T_{∞} is the ambient temperature, $ho_{
m nf}$ denotes the density of a fluid, $\sigma_{
m f}$ denotes the electrical conductivity of the base fluid, $\sigma_{\rm nf}$ denotes the electrical conductivity of nanofluid, $\rho_{\rm f}$ denotes the density of the base fluid, μ_f denotes the viscosity of the base fluid, $\mu_{\rm nf}$ denotes the dynamic viscosity of the nanofluid, B_0 is the applied magnetic field, α is the inclination angle, λ is the latent heat of fluid, C_b is the inertia coefficient, C_1 and β denote the material factor, C_s is the heat capacity of solid surface, K_{nf} represents the thermal conductivity of nanofluid, $(C_p)_{nf}$ denotes the specific heat of nanofluid, $\beta(y)$ and K(y) are, respectively, variable porosity and permeability of porous medium, Q_0 denotes the heat generation/absorption coefficient, d and d_1 are the dimensionless constants, σ_s and K_s are the electrical and thermal conductivity of the nanoparticles respectively, and ρ_s is the density of the nanoparticles. The variable porosity and permeability are given as [35,37]

$$\beta(\eta) = \beta_0(1 + de^{-\eta}), K(\eta) = K_0(1 + d_1e^{-\eta}),$$

where β_0 denotes the porosity at the boundary layer and K_0 denotes the permeability at the boundary layer.

The above partial differential equations (PDEs) are transformed into ordinary differential equations (ODEs) by using the similarity transformations listed below:

$$\eta = y \sqrt{\frac{a}{v_f}}, \ u = axf'(\eta), \ v = -\sqrt{av_f} \ f(\eta),$$

$$\theta(\eta) = \frac{T - T_{\rm m}}{T_{\rm m} - T_{\rm 0}}.$$
(6)

Continuity Eq. (1) satisfies, while Eqs (2) and (3) become

 $(B_2 + \varepsilon) f'''(n) - \varepsilon \delta f''^2(n) - B_1 [f'^2(n) - f(n)f''(n)]$

$$-B_{3} \text{Ha } \sin^{2}(\alpha)[f'(\eta) - A] + A^{2}$$

$$-\frac{B_{2}}{\sigma \text{ Re}} \frac{(1 + de^{-\eta})}{(1 + d_{1}e^{-\eta})} f'(\eta) \qquad (7)$$

$$-\beta^{*} B_{1} \frac{(1 + de^{-\eta})^{2}}{\sqrt{(1 + d_{1}e^{-\eta})^{2}}} f'^{2}(\eta) + Qe^{(-\vartheta\eta)} = 0,$$

$$B_{5}\theta''(\eta) - B_{4} \text{Pr}[S_{1}f'(\eta) + f'(\eta)\theta(\eta) - \theta'(\eta)f(\eta)]$$

$$+ \text{Ec Pr}\Big[(B_{2} + \varepsilon)f''^{2}(\eta) - \frac{1}{3}\varepsilon \delta f''^{4}(\eta)\Big] \qquad (8)$$

$$+ B_{3} \text{ Ha. EcPrsin}^{2}(\alpha)(f'(\eta) - A)^{2} + \delta_{1} \text{Pr}\theta(\eta) = 0.$$

Boundary conditions in the dimensionless form are

$$f'(0) = 1; f'(\infty) = A; \theta(0) = 0; \theta(\infty) = 1 - S_1,$$
 (9)

$$\Pr f(0) + \frac{B_5}{B_1} M\theta'(0) = 0, \tag{10}$$

where Ha represents the magnetic factor, M denotes the melting parameter, Ec is the Eckert number, Pr is the Prandtl number, ε and δ denotes the material factors, S_1 is the stratified thermal parameter, and A is the ratio of free stream velocity to stretching velocity. These parameters are represented below:

$$\begin{aligned} &\text{Ha} = \frac{\sigma_{\text{f}} B_{0}^{2}}{\rho_{\text{f}} c}; \ M = \frac{(C_{\text{p}})_{\text{f}} (T_{\infty} - T_{0})}{\lambda + C_{\text{s}} (T_{\text{m}} - T_{0})}; \\ &\text{Ec} = \frac{U_{\text{w}}^{2}}{(C_{\text{p}})_{\text{f}} (T_{\infty} - T_{0})}; \ \text{Pr} = \frac{(\mu C_{\text{p}})_{\text{f}}}{K_{\text{f}}}; \ \varepsilon = \frac{1}{\beta C_{1} \mu_{\text{f}}}; \\ &\delta = \frac{U_{\text{w}}^{2} C}{2 \nu_{\text{f}} C_{1}^{2}}; \ S_{1} = \frac{d_{1}}{d_{2}}; A = \frac{b}{a}; \\ &B_{1} = (1 - \phi) + \varphi \frac{\rho_{\text{s}}}{\rho_{\text{f}}}; \ B_{2} = (1 - \varphi)^{-2.5}; \ B_{3} = \frac{\sigma_{\text{nf}}}{\sigma_{\text{f}}}; \\ &B_{4} = (1 - \phi) + \varphi \frac{(\rho C_{\text{p}})_{\text{s}}}{(\rho C_{\text{p}})_{\text{f}}}; \ B_{5} = \frac{K_{\text{nf}}}{K_{\text{f}}}; \\ &\rho_{\text{nf}} = (1 - \varphi)\rho_{\text{f}} + \varphi \rho_{\text{s}} \ \mu_{\text{nf}} = (1 - \varphi)^{-2.5} \mu_{\text{f}} \\ &(\rho c_{\text{p}})_{\text{nf}} = (1 - \varphi)(\rho c_{\text{p}})_{\text{f}} + \varphi(\rho c_{\text{p}})_{\text{s}}; \\ &\frac{k_{\text{nf}}}{k_{\text{f}}} = \frac{(k_{\text{s}} + 2k_{\text{f}}) - 2\varphi(k_{\text{f}} - k_{\text{s}})}{(k_{\text{s}} + 2k_{\text{f}}) + \varphi(k_{\text{f}} - k_{\text{s}})}; \\ &\text{and} \ \frac{\sigma_{\text{nf}}}{\sigma_{\text{f}}} = \frac{(\sigma_{\text{s}} + 2\sigma_{\text{f}}) - 2\varphi(\sigma_{\text{f}} - \sigma_{\text{s}})}{(\sigma_{\text{s}} + 2\sigma_{\text{f}}) + \varphi(\sigma_{\text{f}} - \sigma_{\text{s}})}. \end{aligned}$$

The following form is used to analyze the local Nusselt number and skin friction coefficient:

$$Nu_x = \frac{xq_w}{k_f(T_\infty - T_m)}$$
 and $C_f = \frac{\tau_w}{\rho_{nf}U_w^2}$,

where q_{w} represents the heat flux and au_{w} represents the wall shear stress and

$$\tau_{\rm w} = \left(\mu_{\rm nf} + \frac{1}{\beta C_1}\right) \left(\frac{\partial u}{\partial y}\right) - \left(\frac{1}{6\beta C_1^3}\right) \left(\frac{\partial u}{\partial y}\right)^3 \quad \text{and} \quad q_{\rm w} = -k_{\rm nf} \left(\frac{\partial T}{\partial y}\right)$$
as $y \to 0$.

The above quantities in unit less form are as follows:

$$C_{\rm f} \operatorname{Re}_{x}^{1/2} = (B_2 + \varepsilon)f''(0) - \frac{1}{3}\varepsilon \delta f''^3(0)$$
 and,

$$\operatorname{Nu}_{x} = -\frac{B_5\theta'(0)}{\operatorname{Re}_{x}^{-1/2}(1 - s_1)},$$

The following form represents the local Reynolds number: $Re_x = \frac{U_w x}{v_f}$ (Table 2).

3 Methodology (homotopy analysis method, HAM)

In 1992, Liao was the one who initially proposed using the homotopy method. Finding nonlinear model solutions using the homotopic method is the recommended approach. In contrast to past perturbations and non-perturbative processes, the homotopy assessment approach allows us to quickly adjust to new circumstances and change the convergence position and the charges associated with previously learned approximations. In a nutshell, the homotopy evaluation comes with the following additional benefits: It is valid even if a particular nonlinear issue does not contain any little or extended parameters at all, and it can provide us with a straightforward approach to adjust and manipulate the convergence place and charge of estimation collection when it is required to do so. Selecting particular units of base functions allows one to guess the solution to a nonlinear issue using this method.

3.1 Limitations of HAM

HAM is a powerful mathematical technique for solving nonlinear differential equations. Like any method, it is not without its flaws. The main problems with using HAM are:

- 1) It is important to note that the HAM series solution will not necessarily converge in response to all types of problems. There is a remote possibility that the series will not converge at all or will only converge extremely slowly, resulting in findings that are either erroneous or irrelevant. The behavior of convergence is impacted both by the structure of the problem and by the auxiliary linear operator that is chosen.
- 2) The auxiliary linear operator and the initial approximation are responsible for a sizeable portion of the HAM solution's overall effect. The combination of these parameters can be chosen arbitrarily to yield a wide range of results. No systematic procedure can be followed to arrive at the perfect numbers, and it could be challenging.
- 3) The HAM model has the potential to have a high computational complexity, particularly for problems involving many nonlinear components. Calculating the coefficients of the series solution could take a significant amount of time and require a great deal of computer resources.
- 4) HAM may experience difficulties addressing singularities in the problem domain, such as poles or essential

Table 2: Characteristics of nanoparticles and base fluid are illustrated below [18,38]

Physical properties	Base fluid (blood)	Nanoparticles (magnesium)
$\sigma(\mathbf{S} \cdot \mathbf{m}^{-1})$ $C_{\mathbf{p}}(J \cdot \mathbf{kg} \cdot \mathbf{K}^{-1})$	0.18 3,594	2.3 × 10 ⁷ 1046.7
ρ (kg · m ⁻³) k(w· m· K ⁻¹)	1,053 0.492	1,738 156

singularities. Singularities can change the behavior of the series solution as it converges and requires a specific approach.

- 5) HAM can only be used in certain situations. It best solves differential equations with few or no dimensions or disturbances. It might not work well for problems with a lot of or strong nonlinearity. Although HAM has been successfully applied to problems involving just a single dimension, the higher the dimensions, the greater the complexity and computational power required.
- 6) The HAM does not have a trustworthy mechanism for estimating or preventing mistakes, hence it cannot do a rigorous error analysis. It may be challenging to evaluate the accuracy or dependability of the answers that have been found.

Despite these limitations, the HAM is an effective tool for dealing with a wide variety of nonlinear problems. The scientific community is continually developing novel variants and improvements to address some of these limitations and expand the method's scope of applicability. The analytical solution to the higher-order ODEs can be obtained using the homotopy analysis approach in Mathematica 13. The following is an explanation of what is meant by initial hunches and linear operators:

$$f_0(\eta) = A\eta + (1 - A)(1 - e^{-\eta}) - \frac{B_5}{B_1} \left(\frac{M(1 - S_1)}{\text{Pr}} \right), \quad (11)$$

$$\theta_0(\eta) = (1 - S_1)(1 - e^{-\eta}),$$

$$\Xi_f(f) = \frac{\mathrm{d}f^3}{\mathrm{d}\xi^3} - \frac{\mathrm{d}f}{\mathrm{d}\xi}, \ \Xi_{\theta}(\theta) = \frac{\mathrm{d}\theta^2}{\mathrm{d}\xi^2} - \theta, \tag{12}$$

with

$$\Xi_f(J_1 + J_2 e^{-\eta} + J_3 e^{\eta}) = 0, \tag{13}$$

$$\Xi_{\theta}(J_{4}e^{-\eta} + J_{5}e^{\eta}) = 0, \tag{14}$$

where $J_n(n = 1, 2...5)$ are constants.

The final solution f_m , θ_m in terms of corresponding solutions f_m^Λ , θ_m^Λ are written as

$$f_m(\eta) = f_m^{\Lambda}(\eta) + J_1 + J_2 e^{-\eta} + J_3 e^{\eta}, \tag{15}$$

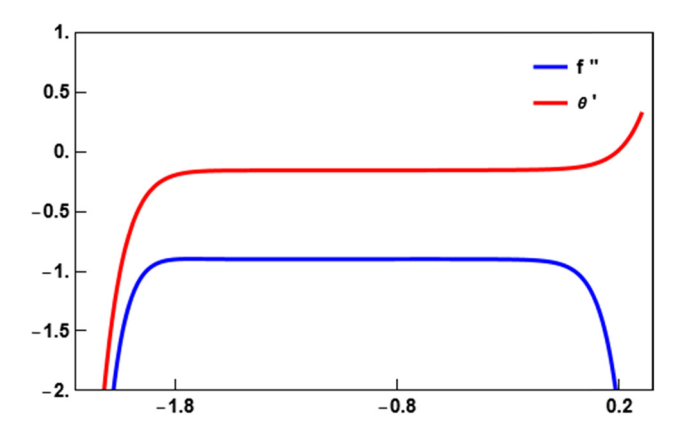
$$\theta_m(\eta) = \theta_m^{\Lambda}(\eta) + J_4 e^{-\eta} + J_5 e^{\eta}. \tag{16}$$

3.2 Convergence analysis

In this subsection, we study the convergence criterion of the method for the above problem. The convergence area occurs parallel to the h-axis, as depicted in Scheme 2. So, the convergence zone for velocity profile is $-1.9 \le h \le -0.1$ while for temperature, the convergence area is $-1.8 \le h \le 0.1$.

4 Parametric study

The main goal of this part is to look at how some important factors, like velocity and temperature field, behave physically and graphically. The dimensions of Powell-Evring fluid parameters are ε and δ in this case. Blood has a value of 1,345 for ε . While δ is not always the same because it changes with stretching [39]. Figure 1 shows what happens to the $f'(\eta)$ of a nanofluid when we change ratio parameter A. The fluid's thickness is analyzed and displayed to be opposing the velocity of A. Additionally, the velocity limit layer's thickness exhibits the same stretching and recessive behavior as the fluid's free stream velocity. When the velocity of the fluid and its surface are equal for A = 0.8, there is no boundary layer present. For A < 0.8, the fluid thickness is greater near the wall, resulting in a higher velocity at the surface. Conversely, for A > 0.8, the fluid thickness is greater outside the wall, resulting in a higher velocity away from the surface. The stagnation point is where the fluid velocity decreases due to the thickness caused by inflammation on the inner walls of the arteries or the point at which veins are obstructed. This can lead to reduced blood



Scheme 2: Convergence curve for velocity and temperature.

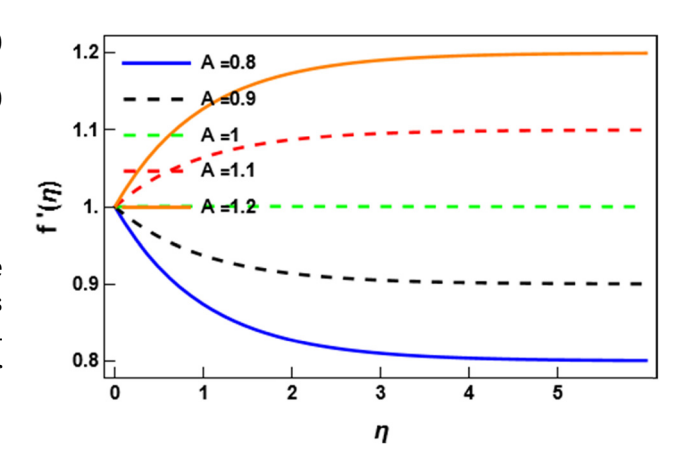


Figure 1: Velocity field for various values of *A*.

circulation within arteries. Whereas with such blockages, fluid velocity reaches its highest level, leading to a thickness or heart attack.

We can find these blocked arteries using variations in graphs. Figure 2 shows how α changes the speed field of a nanofluid made of blood and magnesium. As the angle of slope goes up, the velocity field goes down. This makes both the Lorentz force and magnetic field bigger. So, this force fights against the flow of blood and slowly declines. Due to the slow transfer of nanofluid, patients with hypomagnesemia take a long time to get better. A magnetic field could be made at the injury site to draw the highest amount of magnesium particles there and speed up the healing process.

Figure 3 shows how inertial parameters β affect velocity dispersion. We investigated how inertia causes velocity to increase because a porous media presents increased flow resistance. Figure 4 shows how M affects the velocity field for a blood magnesium nanofluid. As the melting parameter, M, is raised, both $f'(\eta)$ and the wall layer's improve. Because of the dominant melting parameter, there is more convective flow toward a cooling surface. Because of this, the velocity field increases. It is useful for removing things like plaque or fats from the inside walls of veins. The characteristics of the nanofluid volume fraction parameter ϕ on the velocity outline are shown in Figure 5. As ϕ increases, it becomes clear that the velocity decreases. It makes physical sense since nanoparticles speed up the heat transfer rate, which boosts the convective motion of nanofluid. So, the speed goes down gradually. This shows that people with a lack of magnesium get better quickly when they get more magnesium nanoparticles. As can be seen in Figure 6, the horizontal velocity of the nanofluid is affected by the magnetic parameter Ha. The boundary layer's thickness and velocity contour both decrease when magnetic factor Ha increases. Lorentz force

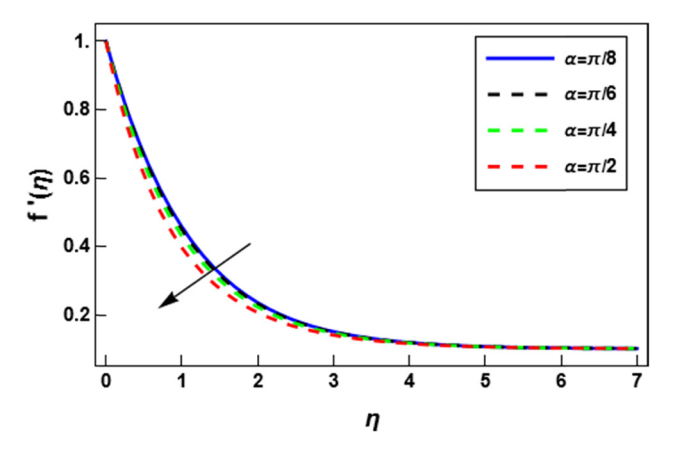


Figure 2: Velocity field for various values of α .

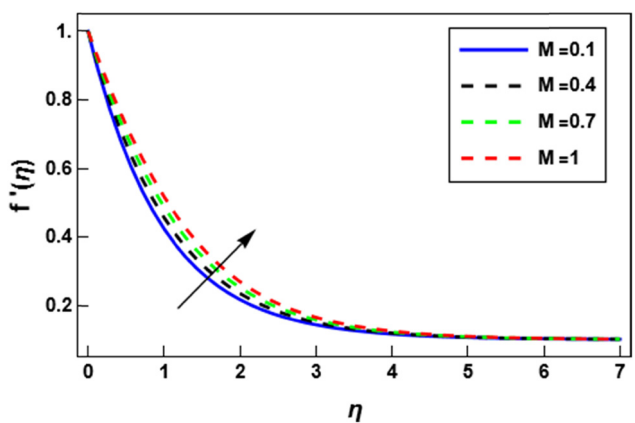


Figure 4: Velocity field for various values of M.

creates retarding forces that act as drag forces in the direction opposite to the flow, making this a physical reality. As a result, less blood flows. Figures 7 and 8 depict the effects of uniform/variable porosity and permeability on velocity distribution. The velocity distribution decreases with the increase in porosity, while increases with the increase in the uniform/variable porosity.

For the nanofluid blood-magnesium, the influence of Ec on $\theta(\eta)$ is depicted in Figure 9. The temperature distribution steadily improves as the Eckert number increases. Forces of repulsion between particles in a fluid are responsible for this behavior because they transform mechanical momentum into thermal energy. This causes the temperature field to expand. The influence of Ha, the magnetic factor, on the nanofluid $\theta(\eta)$ is shown in Figure 10. The temperature profile increases as the magnetic factor is varied. Additionally, the heat transfer boundary layer increases as time passes. Because of this, blood flow becomes more resistant, and heat is produced. Therefore, the temperatures of individual blood cells are raised. Figure 11 shows how the

melting factor, M affects the temperature contour for a blood-based magnesium nanofluid. As the melting value goes up, the temperature value becomes a function that goes down. When the melting value goes up, the thermal border layer gets thicker. Physically, a larger melting parameter makes it easier for heat to move faster from the heated liquid to the cold wall. This means that more heat is lost to the environment, which causes the temperature to drop. Also, when there is a further transfer of heat to the top of veins, fats or plaques on the inside walls melt. So, more melting makes the obstacle to blood flow smaller.

Figure 12 shows how the volume fraction ϕ changes as the temperature changes. It is important to note that when the nanofluid has high numbers, the temperature goes up. Physically, this is because nanofluids are better at moving heat around. Improving the way heat moves through the body is important for keeping the blood at the right temperature and keeping people from getting problems like thin blood, high blood pressure, hemophilia, and other problems. Figure 13 depicts the thermal stratification

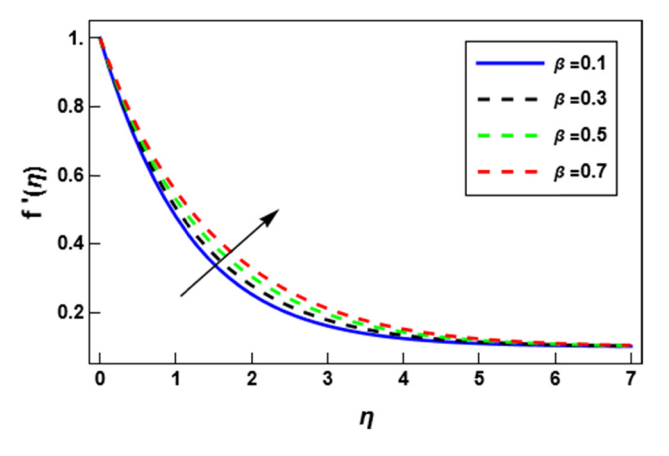


Figure 3: Velocity field for various values of β .

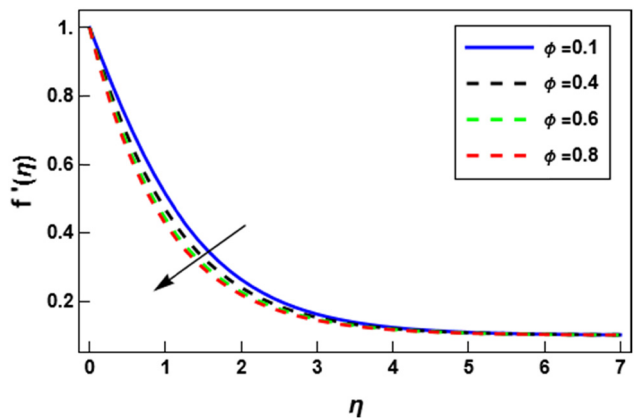
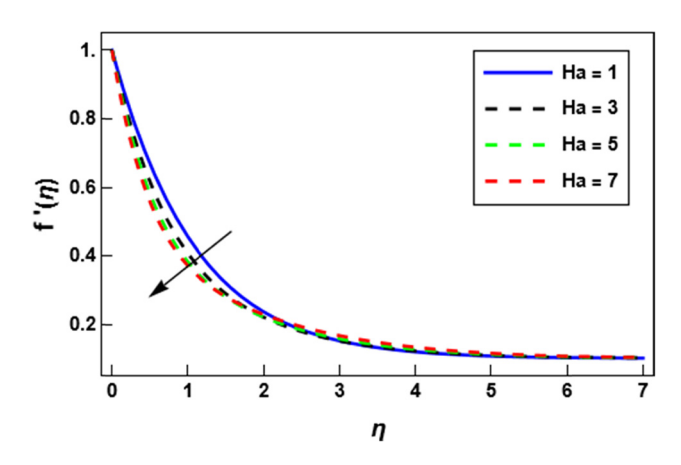


Figure 5: Velocity field for various values of ϕ .

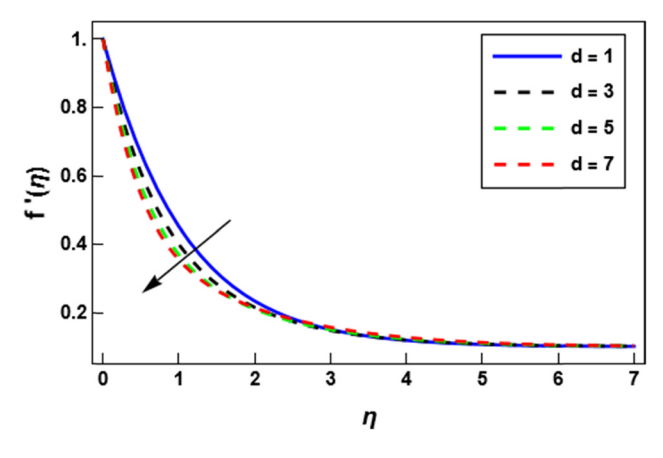


0.8 0.6 Ec= 0.1 Ec= 0.2 0.2 Ec= 0.3 Ec= 0.4 η

Figure 6: Velocity field for various values of Ha.

DE GRUYTER

Figure 9: Temperature field for various values of Ec.



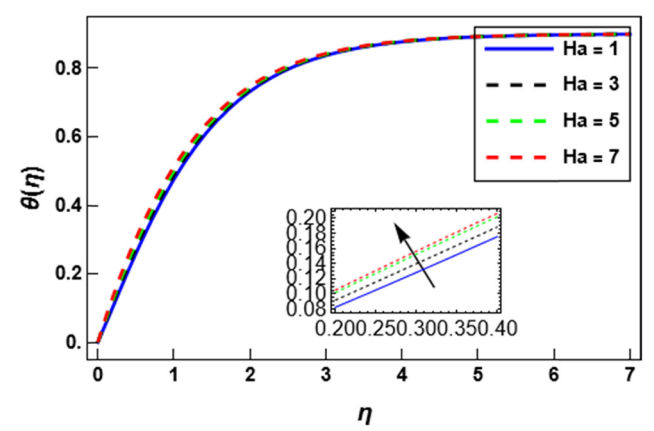
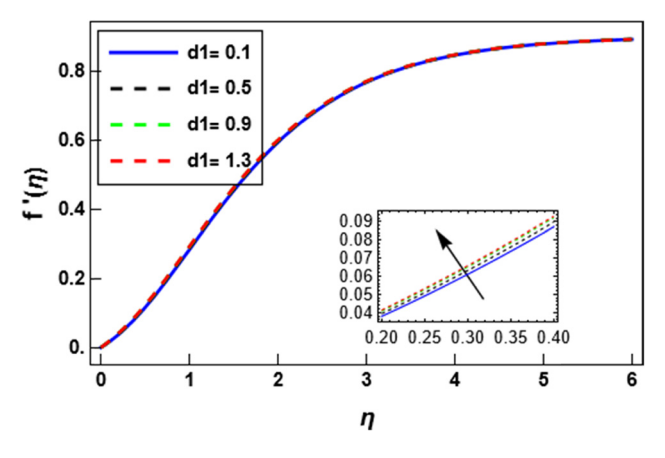


Figure 7: Velocity field for various values of *d*.

Figure 10: Temperature field for various values of Ha.

features on (η) . It can be seen that as the magnitude of s_1 increases, the temperature distribution decreases. As the stratification parameter increases, different density regions prevent heat transport inside the blood. Figure 14 shows how varying thermal conductivity δ affects temperature distribution θ . We looked at whether rising δ causes temperatures to rise. Greater thermal conductivity is correlated with larger δ , which improves the temperature profile.



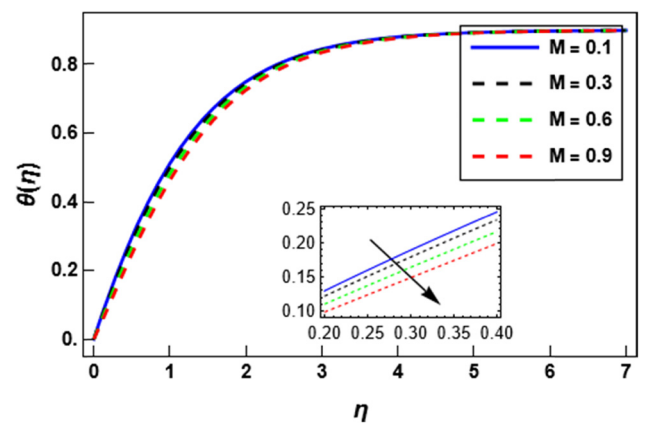


Figure 8: Velocity field for various values of d_1 .

Figure 11: Temperature field for various values of M.

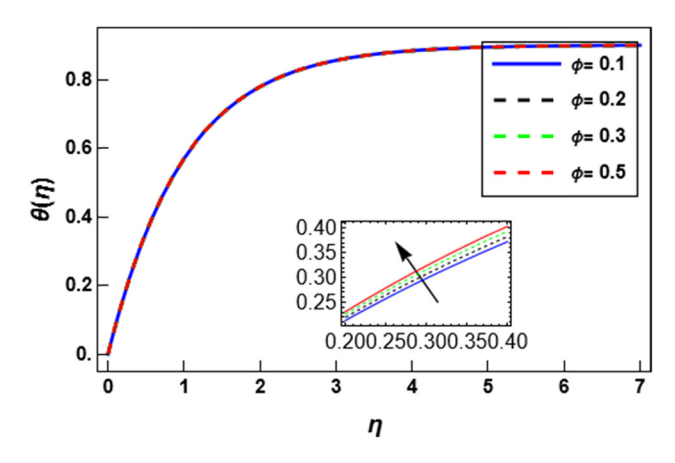


Figure 12: Temperature field for various values of ϕ .

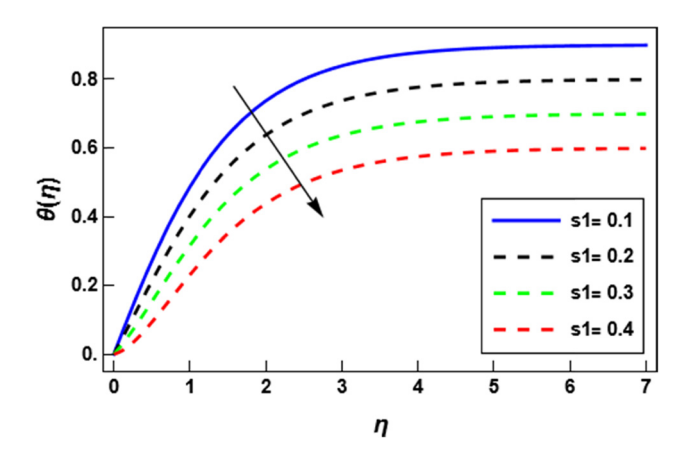


Figure 13: Temperature field for various values of s_1 .

Figure 15 shows that as the ratio parameter increases, the skin friction also increases. Figure 16 shows that as the melting parameter increases, the skin friction coefficient decreases. Figure 17 shows that as the stratification parameter increases,

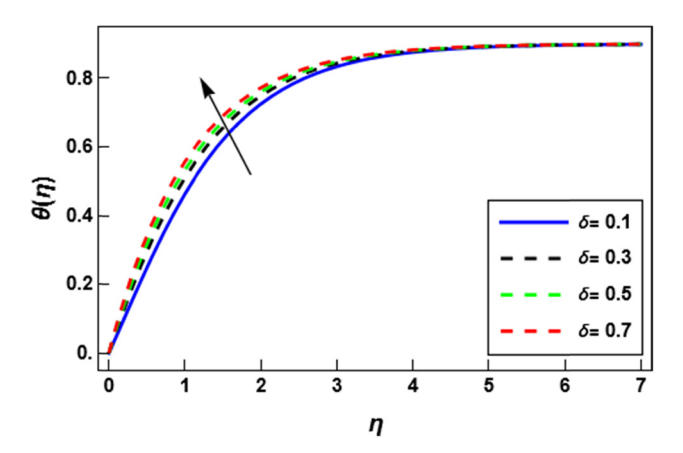


Figure 14: Temperature field for various values of δ .

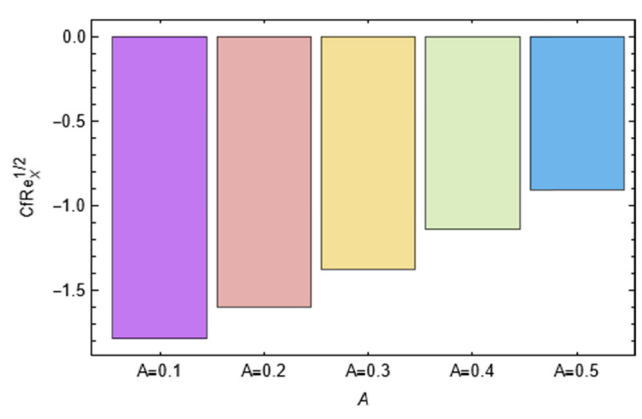


Figure 15: Skin friction for ratio parameter A.

the local Nusselt number decreases. Figure 18 shows that as the Eckert number increases, the local Nusselt number increases. Figures 19 and 20 demonstrate the comparison of present work with the existing literature of Rehman *et al.*'s [3] velocity and temperature fields. In the absence of volume fraction parameter, porosity, and permeability parameters, one can get

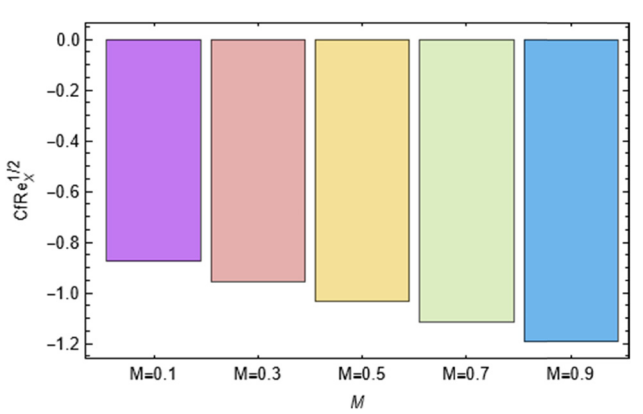


Figure 16: Skin friction for melting parameter M.

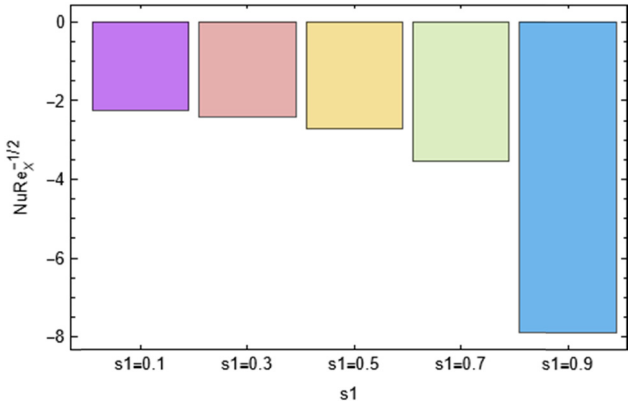


Figure 17: Local Nusselt number for stratification parameter s_1 .

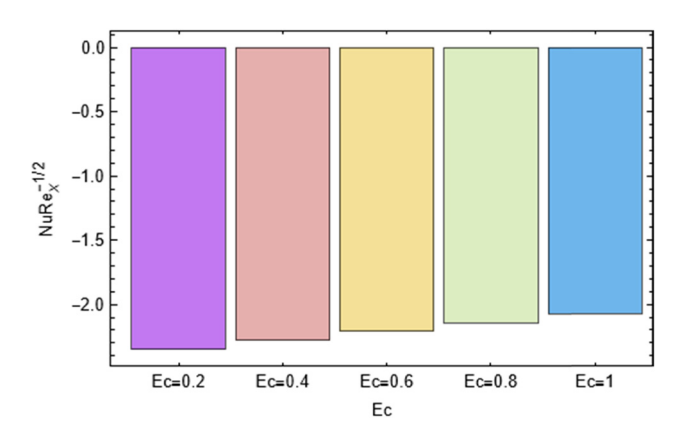


Figure 18: Local Nusselt number for Eckert number Ec.

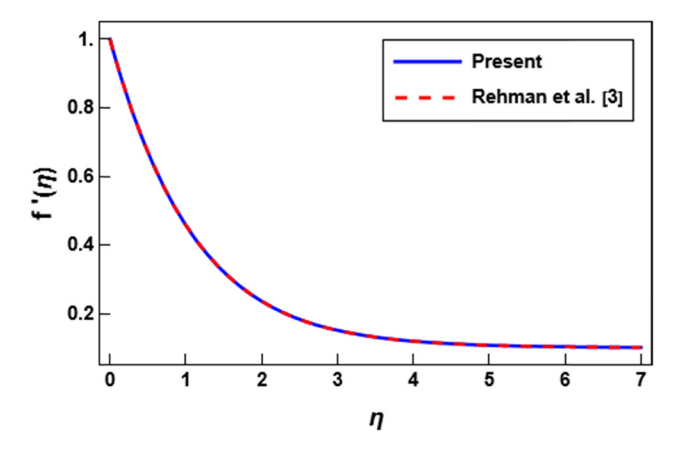


Figure 19: Velocity field of present work and that of Rehman et al. [3].

solution of velocity and temperature fields similar to that of Rehman *et al.* [3].

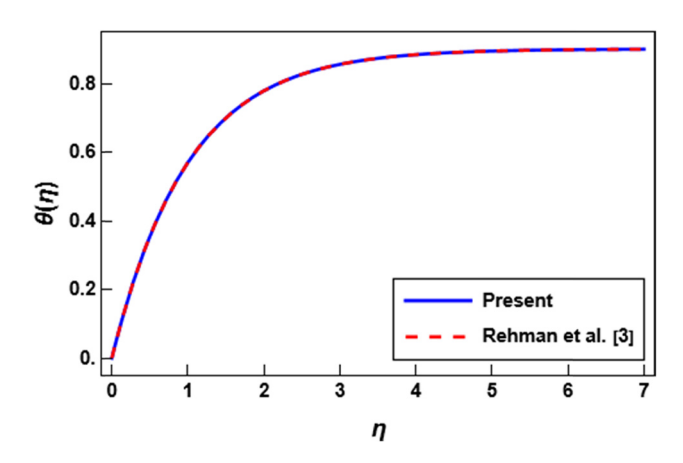


Figure 20: Temperature field of present work and that of Rehman *et al.* [3].

5 Conclusion

This research demonstrates the impact of melting phenomena and heat transport characteristics under more practical boundary conditions. In the modeled scenario, magnesium nanoparticles are uniformly suspended within a base fluid blood to address deficiencies in the human body and promote recovery. The unique material properties of these nanoparticles, including their thermal conductivity and interaction with the magnetic field, play a critical role in enhancing the treatment efficiency. Their precise engineering aids in achieving a desired thermal equilibrium between the fluid phase and the nanoparticles, thereby optimizing the medical outcome. In our analysis, the Powell-Eyring nanofluid flow at the stagnation point is subjected to an inclined magnetic field, emphasizing the interaction between magnetic responsiveness and nanoparticle dynamics. The given PDEs are adeptly transformed into a more manageable ODE system through the application of the correct similarity transformation. The efficacy of the HAM in this context confirms its suitability for complex simulations in material and medical sciences. The following are the final observations:

- 1) The fluid velocity decreases as the values of inclination angle α and porosity d increases, because when α increases, then the Lorentz forces increase while when the d accelerates, the fluid particles have more paths to follow through the material, this increases the resistance and tortuosity. Similarly, fluid velocity increases as the value of inertial parameters β , melting parameter M and uniform/variable porosity d_1 increase. Due to less resistance between the fluid particles because of the increase in the above parameters, the fluid velocity increases.
- 2) Temperature distribution shows an increasing influence, as the values of Eckert number Ec and magnetic factor Ha increases, because more heat is transferred due to the increase in Ec while due to high resistance force it produces more heat because of the enhancement of Ha. While the temperature distribution shows a decreasing influence, as the values of melting parameter M and thermal stratification s_1 increases.

Acknowledgments: The authors acknowledge that this project was supported by Researchers Supporting Project number (RSP2024R411), King Saud University, Riyadh, Saudi Arabia.

Funding information: This project was supported by Researchers Supporting Project number (RSP2024R411), King Saud University, Riyadh, Saudi Arabia.

Author contributions: Haider Raza: conceptualization, design, data interpretation; Sohail Farooq: methodology and experimental validations; Sobia Sattar: data curation and initial draft; Sadique Rehman: writing and validation; Aamir Farooq: project administration, software, and manuscript oversight; Muhammad Kamran: experimental setup and data collection; Mansoor Alshehri: funding and manuscript revisions; and Nehad Ali Shah: theoretical framework and formal analysis. All authors have accepted responsibility for the entire content of this manuscript and approved its submission.

Conflict of interest: The authors state no conflict of interest.

References

- [1] Jabeen, I., M. Farooq, M. Rizwan, R. Ullah, and S. Ahmad. Analysis of nonlinear stratified convective flow of Powell–Eyring fluid: Application of modern diffusion. *Advances in Mechanical Engineering*, Vol. 12, No. 10, 2020 Oct, id. 1687814020959568.
- [2] Lund, L. A., U. Yashkun, and N. A. Shah. Multiple solutions of unsteady Darcy–Forchheimer porous medium flow of Cu–Al₂O₃/ water based hybrid nanofluid with Joule heating and viscous dissipation effect. *Journal of Thermal Analysis and Calorimetry*, 2024 Jan, pp. 1–3.
- [3] Rehman, S., A. Anjum, M. Farooq, and M. Y. Malik. Melting heat phenomenon in thermally stratified fluid reservoirs (Powell–Eyring fluid) with Joule heating. *International Communications in Heat and Mass Transfer*, Vol. 137, 2022 Oct, id. 106196.
- [4] Hatami, M., J. Hatami, and D. D. Ganji. Computer simulation of MHD blood conveying gold nanoparticles as a third grade non-Newtonian nanofluid in a hollow porous vessel. *Computer Methods and Programs in Biomedicine*, Vol. 113, No. 2, 2014 Feb, pp. 632–641.
- [5] Tarakaramu, N., P. V. Satya Narayana, N. Sivakumar, D. Harish Babu, and K. Bhagya Lakshmi. Convective conditions on 3D magnetohydrodynamic (MHD) non-Newtonian nanofluid flow with nonlinear thermal radiation and heat absorption: A numerical analysis. *Journal of Nanofluids*, Vol. 12, No. 2, 2023 Mar, pp. 448–457.
- [6] Shahzad, M., M. Ali, F. Sultan, W. A. Khan, and Z. Hussain. Theoretical analysis of cross-nanofluid flow with nonlinear radiation and magnetohydrodynamics. *Indian Journal of Physics*, Vol. 95, 2021 Mar, pp. 481–488.
- [7] Jeelani, M. B. and A. Abbas. Al₂O₃-Cu\ethylene glycol-based magnetohydrodynamic non-Newtonian Maxwell hybrid nanofluid flow with suction effects in a porous space: Energy saving by solar radiation. Symmetry, Vol. 15, No. 9, 2023 Sep, id. 1794.
- [8] Vinodkumar Reddy, M., M. Ajithkumar, S. S. Zafar, M. Faizan, F. Ali, P. Lakshminarayana. Magnetohydrodynamic stagnation point flow of Williamson hybrid nanofluid via stretching sheet in a porous medium with heat source and chemical reaction. Proceedings of the Institution of Mechanical Engineers, Part E: Journal of Process Mechanical Engineering, 2024. p. 09544089241239583.
- [9] Al-Farhany, K., M. A. Alomari, N. Biswas, A. Laouer, A. M. Abed, and W. Sridhar. Magnetohydrodynamic double-diffusive mixed

- convection in a curvilinear cavity filled with nanofluid and containing conducting fins. *International Communications in Heat and Mass Transfer*, Vol. 144, 2023 May, id. 106802.
- [10] Ganie, A. H., M. M. AlBaidani, S. Farooq, S. Rehman, A. Farooq, F. Z. Duraihem, et al. Computational assessment of thermally stratified magnetohydrodynamics Maxwell nanofluid with Joule heating and melting heat transfer. *Results in Physics*, Vol. 50, 2023 Jul, id. 106542.
- [11] Prasad, P. D., R. K. Kumar, and S. V. Varma. Heat and mass transfer analysis for the MHD flow of nanofluid with radiation absorption. *Ain Shams Engineering Journal*, Vol. 9, No. 4, 2018 Dec, pp. 801–813.
- [12] Chamkha, A. J. and C. Issa. Effects of heat generation/absorption and thermophoresis on hydromagnetic flow with heat and mass transfer over a flat surface. *International Journal of Numerical Methods for Heat & Fluid Flow*, Vol. 10, No. 4, 2000 Jun, pp. 432–449.
- [13] Gorla, R. S., A. Chamkha, and A. M. Rashad. Mixed convective boundary layer flow over a vertical wedge embedded in a porous medium saturated with a nanofluid. *In 2010 3rd International Conference on Thermal Issues in Emerging Technologies Theory and Applications 2010 Dec 19*, IEEE, pp. 445–451.
- [14] Chamkha, A. J. and A. M. Rashad. Natural convection from a vertical permeable cone in a nanofluid saturated porous media for uniform heat and nanoparticles volume fraction fluxes. *International Journal* of Numerical Methods for Heat & Fluid Flow, Vol. 22, No. 8, 2012 Oct, pp. 1073–1085.
- [15] Khan, M., A. Rasheed, M. S. Anwar, and S. T. Shah. Application of fractional derivatives in a Darcy medium natural convection flow of MHD nanofluid. *Ain Shams Engineering Journal*, Vol. 14, No. 9, 2023 Sep, id. 102093.
- [16] Hussain, S., A. Ali, K. Rasheed, A. A. Pasha, S. Algarni, T. Alqahtani, et al. Application of response surface methodology to optimize MHD nanofluid flow over a rotating disk with thermal radiation and Joule heating. *Case Studies in Thermal Engineering*, Vol. 52, 2023 Dec, id. 103715.
- [17] Rafique, K., Z. Mahmood, U. Khan, S. M. Eldin, M. Oreijah, K. Guedri, et al. Investigation of thermal stratification with velocity slip and variable viscosity on MHD flow of Al₂O₃-Cu-TiO₂/H₂O nanofluid over disk. *Case Studies in Thermal Engineering*, Vol. 49, 2023 Sep, id. 103292.
- [18] Lone, S. A., Z. Raizah, M. H. Shah, S. Rehman, A. Saeed, and S. M. Eldin. Thermal and solutal slips impact on 3D-biconvection flow of linearly stratified Casson nanofluid (magnesium-blood) passed over a bi-stretching surface in a rotating frame. *Results in Physics*, Vol. 55, 2023 Dec, id. 107139.
- [19] Kandasamy, R., R. Dharmalingam, and K. S. Prabhu. Thermal and solutal stratification on MHD nanofluid flow over a porous vertical plate. *Alexandria Engineering Journal*, Vol. 57, No. 1, 2018 Mar, pp. 121–130.
- [20] Ahmad, S., S. Nadeem, and M. N. Khan. Mixed convection hybridized micropolar nanofluid with triple stratification and Cattaneo-Christov heat flux model. *Physica Scripta*, Vol. 96, No. 7, 2021 Apr, id. 075205.
- [21] Rehman, K. U., A. Qaiser, M. Y. Malik, and U. Ali. Numerical communication for MHD thermally stratified dual convection flow of Casson fluid yields by stretching cylinder. *Chinese Journal of Physics*, Vol. 55, No. 4, 2017 Aug, pp. 1605–1614.
- [22] Jabeen, I., M. Farooq, and N. A. Mir. Description of stratification phenomena in the fluid reservoirs with first-order chemical reaction. *Advances in Mechanical Engineering*, Vol. 11, No. 4, 2019 Apr, id. 1687814019836897.

- [23] Bilal, S., A. S. Alshomrani, M. Y. Malik, N. Kausar, and F. Khan. Analysis of Carreau fluid in the presence of thermal stratification and magnetic field effect. Results in Physics, Vol. 10, 2018 Sep, pp. 118-125.
- [24] Ellahi, R. The effects of MHD and temperature dependent viscosity on the flow of non-Newtonian nanofluid in a pipe: Analytical solutions. Applied Mathematical Modelling, Vol. 37, No. 3, 2013 Feb, pp. 1451-1467.
- [25] Krishna, M. V., N. A. Ahammad, and A. J. Chamkha. Radiative MHD flow of Casson hybrid nanofluid over an infinite exponentially accelerated vertical porous surface. Case Studies in Thermal Engineering, Vol. 27, 2021 Oct, id. 101229.
- [26] Madhu, M., N. Kishan, and A. J. Chamkha. Unsteady flow of a Maxwell nanofluid over a stretching surface in the presence of magnetohydrodynamic and thermal radiation effects. Propulsion and Power Research, Vol. 6, No. 1, 2017 Mar, pp. 31-40.
- [27] Hafez, N. M., E. N. Thabet, Z. Khan, A. M. Abd-Alla, and S. H. Elhag. Electroosmosis-modulated Darcy-Forchheimer flow of Casson nanofluid over stretching sheets in the presence of Newtonian heating. Case Studies in Thermal Engineering, Vol. 53, 2024 Jan, id. 103806.
- [28] Bhadauria, B. S., A. Kumar, S. K. Rawat, and M. Yaseen. Thermal instability of Tri-hybrid Casson nanofluid with thermal radiation saturated porous medium in different enclosures. Chinese Journal of Physics, Vol. 87, 2024 Feb, pp. 710-727.
- [29] Felicita, A., B. J. Gireesha, B. Nagaraja, P. Venkatesh, and M. R. Krishnamurthy. Mixed convective flow of Casson nanofluid in the microchannel with the effect of couple stresses: irreversibility analysis. International Journal of Modelling and Simulation, Vol. 44, No. 2, 2024 Mar, pp. 91-105.
- [30] Kulkarni, M. and H. F. Shankar. Numerical investigation of mixed convective Williamson nanofluid flow over a stretching/shrinking wedge in the presence of chemical reaction parameter and liquid hydrogen diffusion. Numerical Heat Transfer, Part A: Applications, 2024 Mar, pp. 1-4.

- Reddy, Y. D., F. Mebarek-Oudina, B. S. Goud, and A. I. Ismail. Radiation, velocity and thermal slips effect toward MHD boundary layer flow through heat and mass transport of Williamson nanofluid with porous medium. Arabian Journal for Science and Engineering, Vol. 47, No. 12, 2022 Dec, pp. 16355-16369.
- Akram, S. and Q. Afzal. Effects of thermal and concentration convection and induced magnetic field on peristaltic flow of Williamson nanofluid in inclined uniform channel. The European Physical Journal Plus, Vol. 135, No. 10, 2020 Oct, id. 857.
- [33] Schmidt-nielsen, K. Melting of human fats as related to their location in the body. Acta Physiologica Scandinavica, Vol. 12, No. 2-3, 1946. pp. 123-129
- [34] Nisar, Z., T. Hayat, A. Alsaedi, and B. Ahmad. Wall properties and convective conditions in MHD radiative peristalsis flow of Eyring-Powell nanofluid. Journal of Thermal Analysis and Calorimetry, Vol. 144, 2021 May, pp. 1199-1208.
- [35] Saif, R. S., T. Muhammad, and H. Sadia. Significance of inclined magnetic field in Darcy-Forchheimer flow with variable porosity and thermal conductivity. Physica A: Statistical Mechanics and Its Applications, Vol. 551, 2020 Aug, id. 124067.
- Javed, M. and M. Farooq. Mixed convection and melting rheology in dual stratified Eyring-Powell nanofluid flow over surface of variable thickness: Buongiorno model approach. International Communications in Heat and Mass Transfer, Vol. 125, 2021 Jun, id. 105322.
- [37] Prakash, D., M. Muthtamilselvan, and D. H. Doh. Unsteady MHD non-Darcian flow over a vertical stretching plate embedded in a porous medium with non-uniform heat generation. Applied Mathematics and Computation, Vol. 236, 2014 Jun, pp. 480-492.
- [38] Farooq, M., A. Anjum, S. Rehman, and M. Y. Malik. Entropy analysis in thermally stratified Powell-Eyring magnesium-blood nanofluid convection past a stretching surface. International Communications in Heat and Mass Transfer, Vol. 138, 2022 Nov, id. 106375.
- [39] Bessonov, N., A. Segueira, S. Simakov, Y. Vassilevskii, and V. Volpert. Methods of blood flow modelling. Mathematical modelling of natural phenomena. 2016;11(1):1-25.